Physical modelling of structural and biological soil reinforcement

Knappett, Jonathan

Published in:
Physical Modelling in Geotechnics

DOI:
10.1201/9780429438646

Publication date:
2018

Document Version
Peer reviewed version

Author Accepted Manuscript version of Knappett, J 2018, Physical modelling of structural and biological soil reinforcement. in A McNamara, S Divall & R Goodey (eds), Physical Modelling in Geotechnics: Proceedings of the 9th International Conference on Physical Modelling in Geotechnics (ICPMG 2018), July 17-20, 2018, London, United Kingdom. vol. 1, Taylor & Francis, pp. 87-100, 9th International Conference on Physical Modelling in Geoetchnics, London, United Kingdom, 17/07/18. https://doi.org/10.1201/9780429438646

Physical modelling of structural and biological soil reinforcement

J. A. Knappett
School of Science and Engineering, University of Dundee, UK

ABSTRACT: This paper presents a number of different approaches that can be used to produce small scale models of soil reinforcing elements (here, piles and plant roots) for which similitude of relative soil-structure stiffness and soil-structure strength can be achieved simultaneously. This includes a discussion of the appro-priate dimensionless groups that should be satisfied and a description of the modelling procedures. This is achieved via a series of worked examples of centrifuge model design for steel tubular piles, square reinforced concrete piles and plant roots, though the methods can in principle be applied to other types of reinforcement including retaining walls and soil nails. It is hoped that these will prove to be useful guidance in model design for those new to centrifuge modelling. The modelling procedures demonstrate how principles from materials science can be creatively applied to achieve simultaneous similitude of strength and stiffness, including (i) the use of heat-treatment processing of metal alloys; (ii) development of a micro reinforced concrete based on an understanding of size effect in brittle materials; and (iii) use of materials selection charts for identification of suitable analogue materials. The paper concludes with examples of the application of these procedures in as-sessing the resilience of reinforced slopes to earthquake ground motions using centrifuge modelling to deter-mine whether vegetation (plant roots) can be used as a low-carbon alternative to conventional 'hard' engineer-ing methods for such a problem.

1 INTRODUCTION

There are many geotechnical problems that involve soil-structure interaction. Scaled physical model-ling, particularly using a geotechnical centrifuge, can be used to investigate such problems to (i) improve our understanding of the underlying phenomena for the development of analytical and numerical ap-proaches for engineering design; (ii) provide data for validating such approaches; and (iii) simulate the be-haviour of existing systems to evaluate performance against future actions. In some cases, e.g. where one of the performance requirements for the geotechnical system is that the structural elements must remain elastic, it is sufficient to model only the elastic soil-structure interaction (i.e. ensure similitude of relative soil-structure stiffness). This is often desirable when developing new designs and design methodologies (e.g. cases (i) and (ii) above), where ensuring that the structural elements do not fail prematurely before the soil will normally result in the optimal performance (e.g. minimum deformation) of the system. It is therefore not surprising that elastic similitude (only) has been used in the vast majority of physical model-ling studies conducted to date.

However, in a World with ever-increasing pres-sures on resources and the environment it will be-come increasingly important to extend the life of ex-isting infrastructure where possible. This will necessitate a growing requirement to model the be-haviour of existing systems to assess their perfor-mance against actions beyond that which they were originally designed for. An example is the assess-ment of the performance of reinforcement schemes for slopes subjected to earthquakes or extreme rainfall events where an extension of the design life results in an increase in the size of the design event if the prob-ability of failure is maintained due to an increase in exposure (an effect compounded by climate change in the case of rainfall events). In such cases, behaviour may transition into an inelastic range where it would be desirable to scale relative soil-structure strength to obtain an accurate model of the system's behaviour.

This paper will summarise approaches for producing reduced scale models of structural elements (both in steel and reinforced concrete) which can simultaneously scale stiffness and strength, and therefore simultaneously satisfy the appropriate dimensionless groups to ensure similitude in centrifuge tests. This will be discussed in the context of reinforcement of sloping ground against earthquake actions using a row of discretely-spaced vertical piles. The paper will also summarise an approach to producing representative physical analogues of plant roots using modern 3-D printing techniques (similarly ensuring similitude of both stiffness and strength simultaneously), which could be used as an alternative biological slope reinforcement with much lower cost and lower embodied carbon.

2 SLOPE REINFORCEMENT USING PILES

The example problem of slope reinforcement has been selected as it represents a case where there are two competing failure modes at the ultimate limiting state, namely: (i) the pile is stronger than the soil so that the soil flows around the pile (a geotechnical failure); or (ii) the soil is stronger than the pile, so that the pile suffers a structural failure. These are shown in Figure 1.

In this section, appropriate dimensionless groups

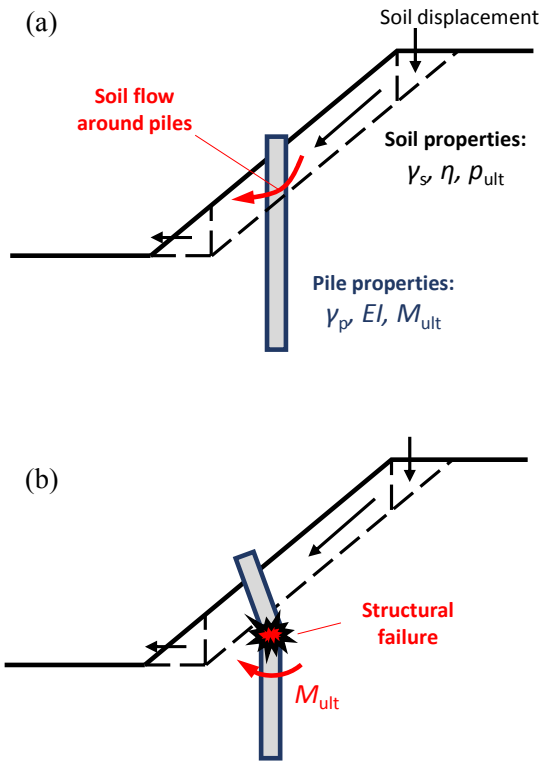

Figure 1 Failure mechanisms of a pile-reinforced slope: (a) soil fails first; (b) pile fails first.

will be presented to achieve similitude of both relative soil-pile stiffness and relative soil-pile strength. These will be used to describe the requirements on the structural models that will be discussed in subsequent sections. In the remainder of the paper, dimensions are represented by M for mass, L for length and T for time.

2.1 *Elastic soil-pile interaction*

An appropriate dimensionless group that can be used to express relative soil-pile stiffness is:

$$\frac{\eta B L_p^4}{EI} \tag{1}$$

after Florres-Berrones & Whitman (1982), where η is the modulus of subgrade reaction (dimensions of $ML^{-2}T^{-2}$), B is the pile width or diameter and L_p a length of the pile (both with dimensions of L), and EI is the pile elastic bending stiffness (dimensions of ML^3T^{-2}).

In a 1:N (model:prototype) scale centrifuge test using the same soil in model and prototype, the soil stress-strain behaviour is scaled 1:1, so η scales as N:1, and EI therefore scales as $1:N^4$ to ensure similitude. This is the conventional scaling law recovered in Wood (2004) or Madabhushi (2014), amongst others, and sets the requirement on the elastic bending stiffness of the model pile.

2.2 *Soil-pile interaction at the ultimate limit state*

Equation 1 represents the relative soil-pile lateral stiffness. To obtain the correct failure mechanism at the ultimate limit state, similitude in the relative soil-pile strength must be achieved to avoid a bias towards one of other mechanism. One possible dimensionless group expresses this in terms of the moment induced in the pile due to the maximum lateral soil pressure at soil failure (M_{sf}) and the structural moment capacity of the pile (M_{ult}):

$$\frac{M_{sf}}{M_{ult}} \tag{2}$$

The soil term in Equation 2, M_{sf}, can be approximated be considering the free body diagram shown in Figure 2. The maximum lateral earth pressure, p_{ult}, for a soil with a drained response (as an example) is:

$$p_{ult}(z) = 3K_p \cdot (\gamma' z) \cdot B \tag{3}$$

where γ'_s is the effective (buoyant) unit weight of the soil, z is the depth below the ground surface and K_p is the passive earth pressure coefficient. Therefore, by taking moments about the intersection of the slip plane with the pile when the slip plane is at a depth $z = L_a$ (active length):

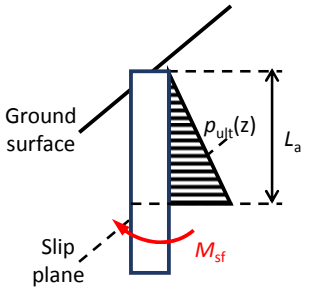

Figure 2 Free-body diagram for a pile subject to lateral pressure from plastically-yielding soil.

$$M_{sf} = \frac{3K_p\gamma'_s BL_a^3}{6} \quad (4)$$

Combining Equations 2 and 4 suggests that a suitable dimensionless group for relative soil-pile strength is:

$$\frac{K_p\gamma'_s BL_a^3}{M_{ult}} \quad (5)$$

K_p has no dimensions, while unit weight has dimensions of $ML^{-2}T^{-2}$. Therefore, in a 1:N scale centrifuge test using the same soil in model and prototype, M_{ult} must scale by $1:N^3$ for similitude.

3 MODEL PILE DESIGN – STEEL PILE

From Section 2, it has been shown that for complete similitude in the slope reinforcement problem, any model pile designed for a centrifuge test must have a bending stiffness scaled by $1:N^4$ compared to the prototype and a moment capacity scaled by $1:N^3$. This section will present an example of the design of a model pile at a scale of 1:80 (N = 80) where the prototype is to represent an S355 steel tubular pile (i.e. yield stress f_y = 355 MPa) with outer diameter B = 496 mm and wall thickness t = 20 mm.

It is not practical in this case to produce a geometrically-scaled model pile in the same steel, as the resulting wall thickness would be 0.25 mm. This would be difficult to machine and small flaws in this process could result in significant localised weaknesses in the model pile wall. Indeed, it is common in centrifuge modelling to design a section with larger wall thickness in a material with a lower Young's Modulus so that EI can be appropriately scaled. Aluminium-alloy is a popular material as it is easy to machine and is corrosion resistant. Table 1 presents the results of using 6063-series aluminium alloy to produce the model pile (all values at prototype scale). 'T6' refers to the temper of the material (essentially a series of heat-treatment processes that have been applied during its production).

Table 1 demonstrates that a tube with outer diameter 6.2 mm and wall thickness of 1.4 mm can achieve representative B and EI (within 3% of the target value), satisfying Equation 1. The Young's Modulus of the 6063 alloy is approximately one third that of steel, so the second moment of area (I) has been increased by a factor of approximately three to compensate.

Table 1 Design of a 1:80 scale steel pile in 6000-series aluminium alloy

Parameter (units)	Steel field pile	6063 prototype (T6 / T4 temper)	Prototype/field
B (m)	0.496	0.496	1.00
t (m)	0.02	0.112	N/A
I (m^4)	0.00085	0.00270	3.18
E (GPa)	210	68	0.32
EI (MNm^2)	178	184	1.03
Z_p (m^3)	0.00453	0.01698	3.75
f_y (MPa)	355	250 / 90	0.70 / 0.25
M_{ult} (kNm)	1610	4246 / 1530	2.64 / 0.95

Increasing I, however, also increases the plastic section modulus Z_p (by a factor of nearly four) as these two parameters are both controlled by the geometry of the cross-section. This is problematic as f_y for 6063-T6 is only 70% of that of the steel and the plastic moment capacity is given by:

$$M_{ult} = f_y Z_p \quad (6)$$

Therefore, to simultaneously satisfy Equation 5, the yield stress of the aluminium-alloy needs to be reduced. This can be achieved by using an alloy of a different temper. The commonly available T6 temper is achieved through solution heat treatment (520 °C for one hour followed by water quench) followed by aging (175 °C for 8 hours). The ageing process increases f_y without changing E. A softer temper (T4) is achieved by applying the solution heat treatment without ageing. Table 1 shows that the lower value of f_y = 90 MPa for this un-aged material results in M_{ult} within 5% of the desired prototype value. The values of EI and M_{ult} in Table 1 were validated by conducting four-point bending tests on 200 mm long pile models in both 6063-T6 and 6063-T4 alloys, the results of which are shown in Figure 3.

It should be noted that T4 temper is not commonly available in the sizes of tube that were used to fabricate the model piles. However 6063-T6 machined to the correct dimensions can be annealed followed by heat-treatment to remove the effects of the aging and return the material to T4 temper (for the models presented in Figure 3 this was conducted by Beccles Heat Treatment, UK). It is desirable to do this as cold-working of the material and (a long) storage time will cause ageing of T4 towards the more stable T6 temper, so it is best to perform the heat treatment as the last process before testing.

4 MODEL PILE DESIGN – REINFORCED-CONCRETE PILE

If the piles to be modelled in the centrifuge are instead to represent reinforced concrete (RC) piles in the field, producing a model that can even just satisfy Equation 1 is complicated due to the composite nature of the material and the very different behaviour of the constituent materials (concrete and steel) in compression and tension (Knappett, 2008). It is first necessary to determine the effective (working) stiffness, as *EI* in a reinforced concrete beam is dependent on: (i) the overall section size (as in Section 3); (ii) the Young's Modulii of the concrete and steel; and (iii) the amount of steel reinforcement. In a beam-column (i.e. where there is combined bending and axial load), *EI* is also dependent on (iv) the axial load in the section (this will be discussed further in Section 4.3).

This section will present an example of the design of a model pile at a scale of 1:50 (N = 50) where the prototype is to represent a singly-reinforced square precast RC pile of size B = 500 mm, containing A_s/A_g = 0.85% steel (where A_s is the cross-sectional area of the steel reinforcement, and A_g is the gross area of the section, $A_g = B^2$). Being singly-reinforced, the pile will have the reinforcement all on the upslope side (to resist bending due to lateral earth pressure). The *EI* for a singly-reinforced rectangular RC section can be found using 'transformed area' theory after Kong and Evans (1987):

$$EI = E_c I_g \left[4\left(\frac{x}{B}\right)^3 + 12\left(\frac{E_s}{E_c}\right)\left(\frac{A_s}{A_g}\right)\left(1-\frac{x}{B}\right)^2 \right] \qquad (7)$$

where E_c is the Young's Modulus of the concrete, I_g is the gross second moment of area (= $B^4/12$), x is the depth of the neutral axis (see Figure 4a) and E_s is the Young's Modulus of the steel. Equation 7 assumes that the loads on the beam are expected to induce moments greater than one third of the moment capacity, such that the concrete below the neutral axis that is in tension will be cracked and will therefore not contribute to the stiffness. This is indicated by the diagram in Figure 4a. The depth of the neutral axis is determined for the cracked section when considering the moment capacity of the section, which for a singly-reinforced section is given by:

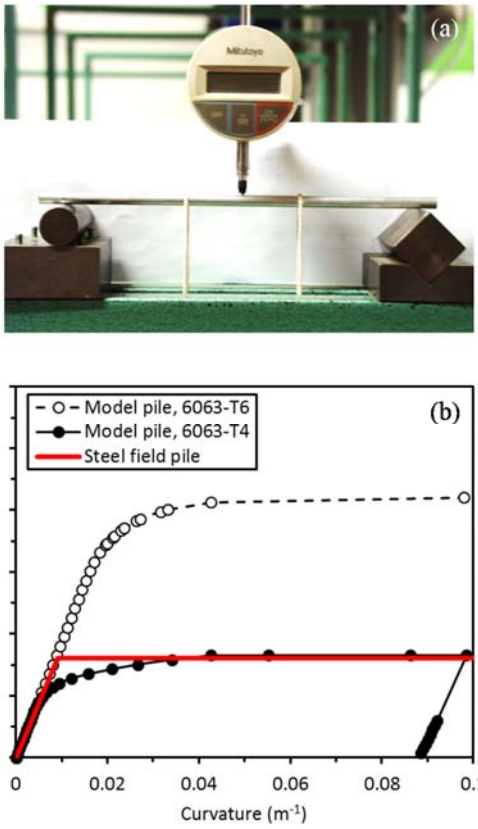

Figure 3 Structural behaviour of 1:80 model steel piles: (a) four-point bending test arrangement; (b) results at prototype scale.

$$\frac{x}{B} = -\left(\frac{E_s}{E_c}\right)\left(\frac{A_s}{A_g}\right) + \sqrt{\left(\frac{E_s}{E_c}\right)^2\left(\frac{A_s}{A_g}\right)^2 + 2\left(\frac{E_s}{E_c}\right)\left(\frac{A_s}{A_g}\right)} \qquad (8)$$

after Kong and Evans (1987). The moment capacity of a singly-reinforced section is given by:

$$M_{ult} = A_s f_y B\left[1-\left(\frac{A_s}{A_g}\right)\left(\frac{f_y}{Kf_c}\right)\right] \qquad (9)$$

where f_c is the concrete compressive strength and K is a stress-block factor (K = 0.6 is assumed herein). If

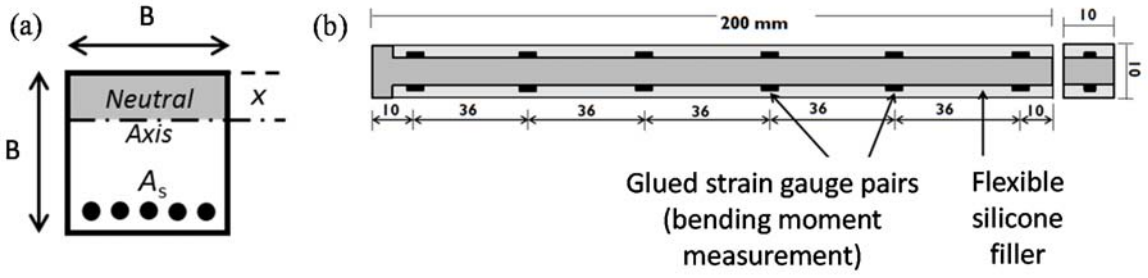

Figure 4 1:50 elastic model of an RC pile: (a) singly-reinforced cracked concrete section (shaded zone in compression); (b) Aluminium-alloy composite section (dimensions in mm at model scale; additional instrumentation also shown).

the pile is circular, an approach to determine *EI* can be found in Knappett (2008).

4.1 *Aluminium-alloy based ('elastic') model pile*

Table 2 presents the results of using 6063-series aluminium alloy (as in Section 3) to produce a model pile that has the same *EI* as the RC section. This was achieved by machining a solid square rod to reduce the depth (*d*), while keeping the same width. Such a section does not have the correct external dimensions at prototype scale, but this can be remedied by using a flexible filler (e.g. silicone) with comparatively negligible stiffness to fill the gap (Figure 4b). Figure 5 shows the construction procedure of such piles, where the composite aluminium-silicone section is wrapped in a thin adhesive and waterproof aluminium tape (to prevent delamination of the filler). Fine sand was subsequently adhered to the surface of the pile using epoxy resin to mimic the rough soil-pile interface typical of concrete.

Table 2 Design of a 1:50 scale RC pile in 6000-series aluminium alloy

Parameter (units)	RC field pile	6063 prototype (T6 / T4 temper)	Prototype/field
B (m)	0.5	0.5	1.00
d (m)	0.5	0.26 (0.5*)	* with silicone
$E_{(c)}$ (GPa)	25	70	2.80
E_s/E_c (-)	8.4	N/A	N/A
A_s/A_g (-)	0.85%	N/A	N/A
EI (MNm^2)	47.7	51.3	1.08
f_c (MPa)	23.5	N/A	N/A
f_y (MPa)	460	250 / 90	0.54 / 0.20
M_{ult} (kNm)	230	3750 / 1350	16.30 / 5.87

While the elastic behaviour (*EI*) can be well approximated by this approach, the moment capacity for the model section at prototype scale (calculated using Equation 6) is greatly over-predicted compared to that of the field RC pile (calculated using Equation 9) irrespective of whether T6 or T4 temper materials are used. Therefore if both Equations 1 and 5 are to be satisfied simultaneously, a new modelling approach is required.

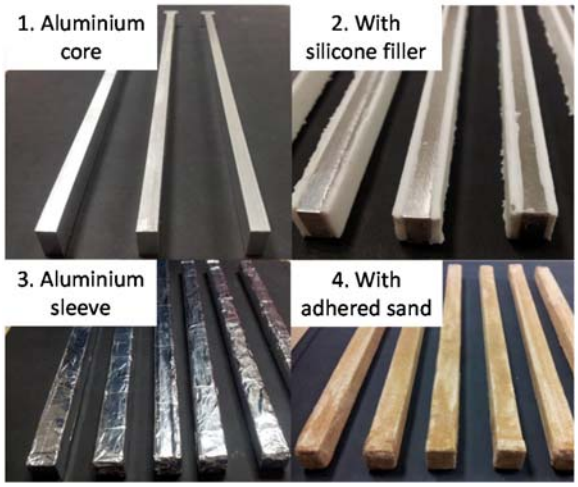

Figure 5 Construction process for aluminium-alloy based 1:50 model RC pile.

4.2 *Scale model reinforced concrete*

An alternative approach to the one outlined in Section 4.1 is to produce a purely geometrically scaled model, i.e. one where the Young's modulus and strength of all of the materials are scaled 1:1, with the concrete element modelled using a brittle model material and the reinforcement modelled using a ductile material. In principle, if this can be achieved then the behaviour of the model section will automatically display similar behaviour to the full scale section. If, as with the soil, the same concrete material is used in the model, the coarse aggregate size in the concrete will become increasingly larger relative to the size of the structural element as N is increased. As the tensile strength of concrete is controlled by the size of cracks/flaws, and their size is approximately proportional to the size of the aggregate (Bažant and Yu, 2005), use of the same material will tend to result in 'over-strength' in the small scale models. Results collated from previous tests on reinforced concrete

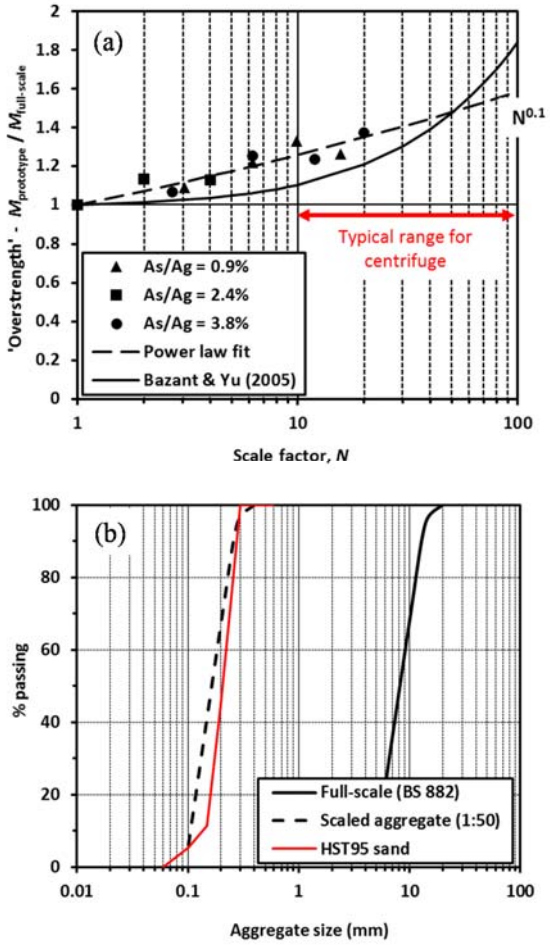

Figure 6 (a) Over-strength observed in previous bending tests of RC beams; (b) approach to geometric scaling of coarse aggregate.

beams at various scales with varying amounts of reinforcement are shown in Figure 6a (after Litle and Paparoni, 1966; Belgin and Sener, 2008).

The model of Bažant and Yu (2005) in Figure 6a suggests that the overstrength should be relatively small over conventional scales used for structural model testing ($1 < N < 10$), but will be unmanageable at scales commonly used in geotechnical centrifuge testing ($N > 10$). A fit to the test data suggests that the over-strength will be worse for $N < 50$. A solution to this is to scale down the particle size of the coarse aggregate proportionally as N increases. HST95 silica sand, commonly used at the University of Dundee for centrifuge modelling of sands (with $D_{10} = 0.15$ mm) represents a suitable material for a common scale of 1:50, as shown in Figure 6b.

This fine sand is mixed with plaster and water to produce a model gypsum mortar (model micro concrete) with representative compressive and tensile strength (assessed via the Modulus of rupture, f_r, i.e. the splitting strength of an unreinforced prism) of field concretes. This is summarised in Figure 7a. Different strengths of model concrete can be achieved by varying the water to plaster ratio, w/p (by mass) and also by using different types of plaster. Plaster comes in two principal forms, alpha-hemihydrate and beta-hemihydrate; the former is a stronger plaster typically used for producing dental moulds (Crystacal D™ from Lafarge Prestia, France was used herein), while the latter form is weaker and normally used in model making (Surgical plaster, also from Lafarge Prestia, France, was used herein). The range shown in Figure 7a can be used to represent weaker mass concretes up to structural grades of concrete. The error bars (based on testing 6 samples of each model micro-concrete in compression and 10 in rupture) indicate that the strength is variable; Figure 7b indicates that this variability is similar to that of well-produced concrete produced in the field. Approximate conversion between cylinder (f'_c) and cube (f_{cu}) compressive strengths can be achieved using:

$$f'_c \approx 0.90 f_{cu} - 6.26 \quad (10)$$

after Mansur and Islam (2002). Further details about the model micro-concrete and the material testing conducted can be found in Knappett et al. (2011).

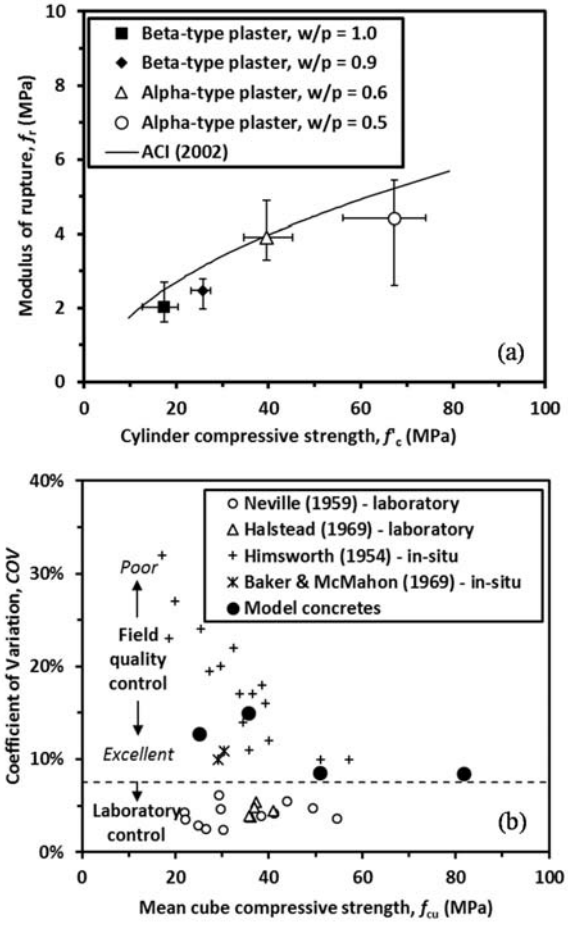

Figure 7 Basic material properties of model micro-concrete: (a) compressive and tensile strength; (b) variability.

Reinforcement can be added to the model concrete by using steel wire to ensure 1:1 scaling of Young's modulus and tensile strength. Modelling conducted to date at the University of Dundee has used two materials – a grade 316 stainless steel cold-drawn wire with $f_y = 460$ MPa and a grade 304 stainless steel cold-drawn wire with $f_y = 380$ MPa. The use of stainless steel prevents corrosion which might split the small model sections (as oxidation products will not scale) but the smooth wires must therefore receive a coating of fine sand using epoxy resin (similar to the surface coating describe in Section 4.1 and shown in Figure 5). This allows a 'rough' bond with the fine sand in the model micro-concrete to approximate the effect of the ribbing on conventional deformed reinforcing bars.

To produce a model RC section, the modelling procedure shown in Figure 8 is followed. A formwork is firstly produced that is bolted together to allow it to be easily taken apart after casting to remove the model piles without damage. This contains small holes at either end that can be used to fix the longitudinal reinforcement and hold it in-place. Shear reinforcement may be added by threading the longitudinal wires through either (i) individually made stirrups (e.g. Loli et al., 2014); or (ii) through a continuous spiral wound around a rectangular former with marks to indicate the required spacing which is tied-off at either end (e.g. Al-Defae and Knappett, 2014). Once the reinforcing cage is fully-formed, the dry materials (sand and plaster) for the model concrete are measured-out and mixed, before the water is added. The plaster begins to harden rapidly, so the mixture is immediately poured into the formwork. The model elements can be de-moulded after 24 hours (though care must be taken as they will be weak at this stage). The models are then left to cure for 28 days.

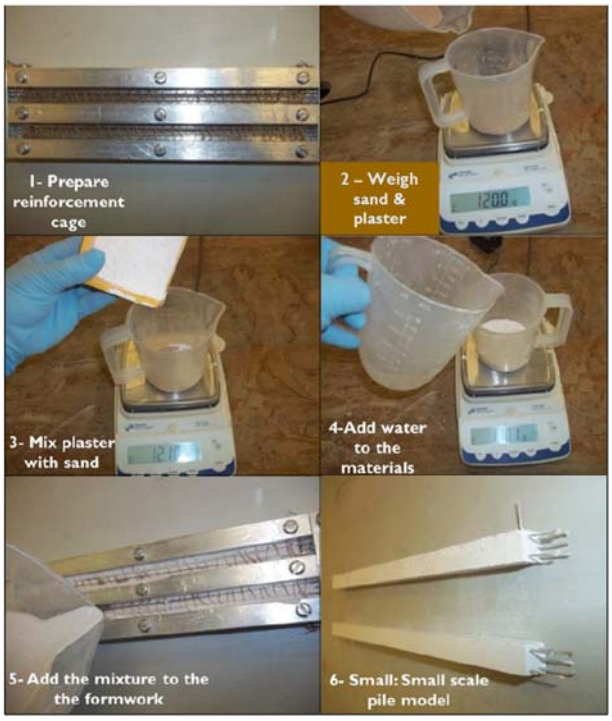

Figure 8 Casting procedure for model RC sections (pile shown).

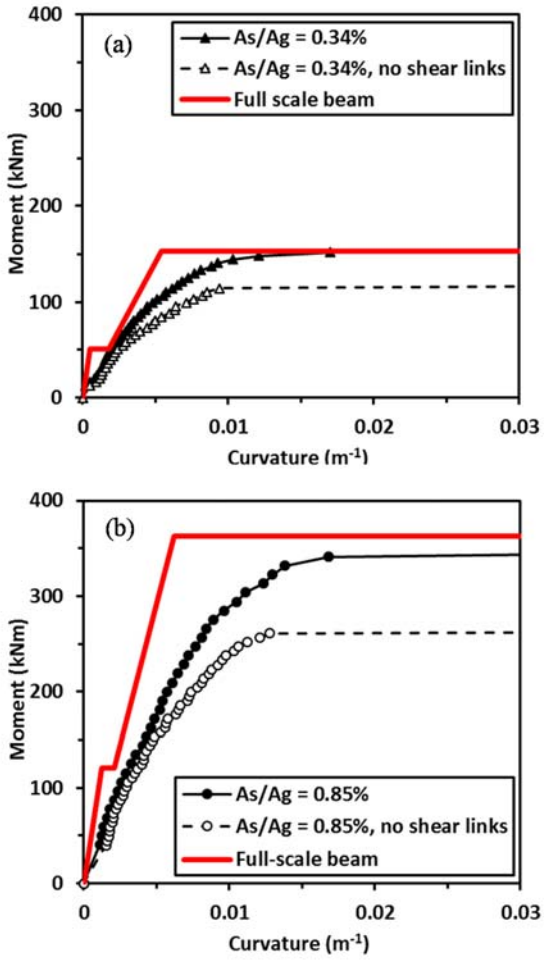

Figure 9 Structural behviour of 1:50 scale model RC piles from four-point bending tests (results at prototype scale).

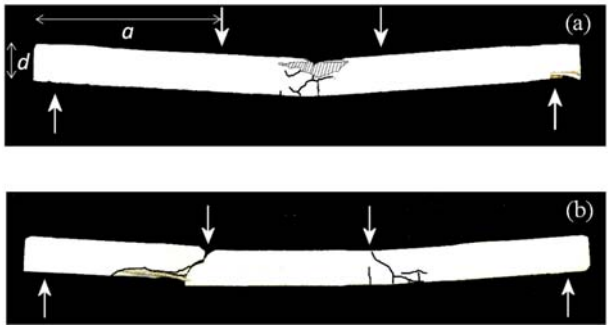

Figure 10 Damage to model RC beams in four-point bending tests (A_s/A_g = 0.85%): (a) bending failure, beam with shear reinforcement; (b) flexural shear failure, beam without shear reinforcement.

Figure 9 presents example results of four-point bending tests on 200 mm long singly-reinforced model concrete beams with different amounts of longitudinal reinforcement (represented by A_s/A_g, in grade 316 wire), both with and without shear reinforcement (a continuous spiral of grade 304 wire, representing 10 mm diameter links at pitch/spacing of 360 mm at prototype scale). So long as a suitable amount of shear reinforcement is included the beams can simultaneously scale the EI and M_{ult} (for the cracked section), and can therefore simultaneously satisfy Equations 1 and 5 for a reinforced concrete section, just as the heat-treated aluminium-alloy tubes achieved for the steel section in Section 3 (c.f. Figure 3b). The failure mechanism for such cases even exhibits tensile cracking and compressive spalling, as in full-scale RC beams; this is shown in Figure 10a. Furthermore if the shear reinforcement is removed a lower capacity is obtained in Figure 9 for both steel percentages, associated with a change in failure mechanism to flexural shear (see Figure 10b). This is consistent with the behaviour of RC beams with inadequate shear reinforcement at the shear-span ratio tested (a/d = 5.3 in Figure 10, e.g. Bažant and Yu, 2005).

4.3 *Extension to combined axial load and bending*

Having demonstrated that the model RC can replicate EI, M_{ult} and damage mechanisms in pure bending (which is most appropriate for the slope reinforcement problem), further testing has examined the behaviour of the composite material under combined axial load and bending moment. Achieving similitude under such conditions would make it suitable for use in piled foundation problems where lateral loads are also present (e.g. structural foundations, columns or bridge piers under earthquake loading).

Five doubly-reinforced concrete piles were fabricated as outlined in Section 4.2, with A_s/A_g = 0.66% (in total). These were tested as a vertical fixed-base cantilever with a static vertical load ($0 \le P \le 400$ kN) applied through a load hanger and a lateral worm

screw to apply displacement-controlled lateral loading. The vertical loading resulted in instability of some of the tested sections once the moments had reached half of the expected values (due to P-Δ amplification as the lateral deflections, Δ, became larger). The moment-curvature behaviour up to this point was sufficiently developed to determine EI in all cases; however, only two of the columns reached a stable plastic failure for determination of M_{ult} (those at P = 0 kN and 150 kN). Test data for these cases is shown in Figure 11.

In Figure 11a there is evidence that increasing P increases both EI and M_{ult} of the model RC section. In terms of the strength, this is consistent with a typical RC interaction (P-M) diagram, where moment capacity increases with increasing axial load up to a maximum value before reducing to zero as the axial force approaches its limiting value (the 'squash' load, $P = f'_c A_g$). The interaction diagram for the representative field RC pile was here determined using BS8110 (1997) and part of this (for P < 1 MN) is shown in Figure 11b for comparison with the model RC test data. It is apparent that the model RC appears to capture the interaction behaviour at low values of P, though further testing is clearly required to confirm this result across a wider range of test conditions.

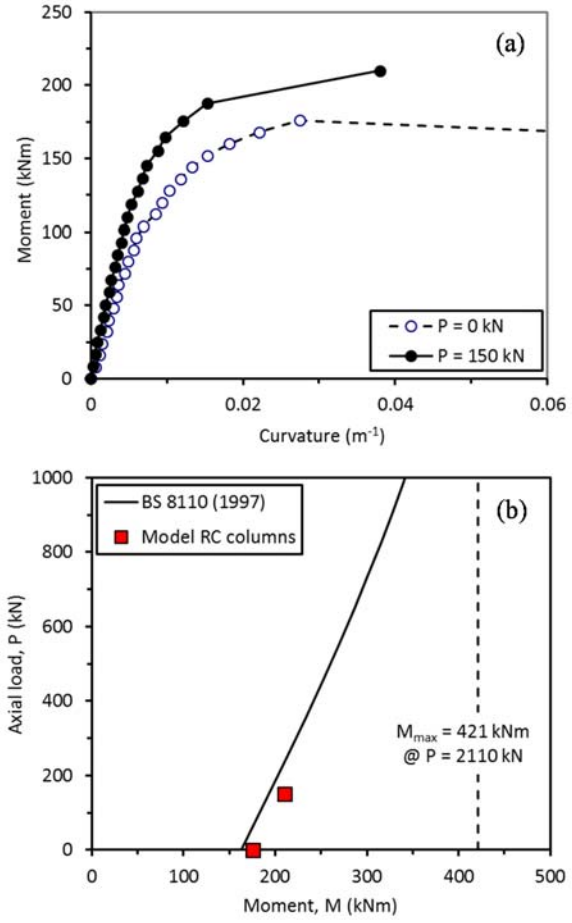

Figure 11 (a) Example behaviour of model columns/piles under combined axial load and bending; (b) interaction diagram.

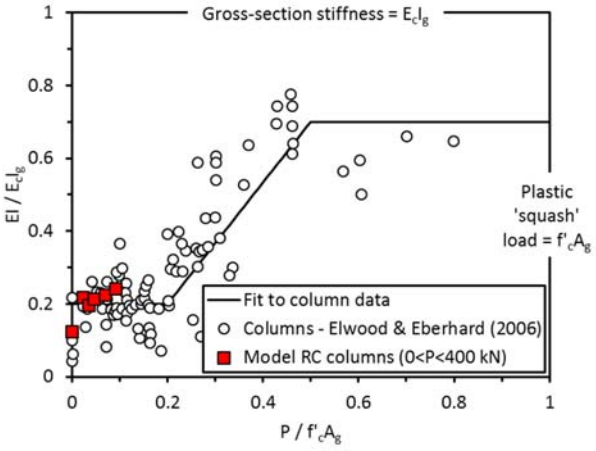

Figure 12 Effect of axial load on bending stiffness of reinforced concrete columns.

Figure 12 shows a comparison of the bending stiffness of the model RC sections tested as a function of axial load, against a database of full scale tests of RC columns (reported by Elwood and Eberhard, 2006). This emphasises the difficulty in scaling the bending stiffness of RC in centrifuge soil-structure interaction models, as (i) $EI < E_c I_g$, as mentioned previously for singly-reinforced beams (see Equation 7); and (ii) EI is further affected non-linearly by the axial load P. It can be seen that the model RC datapoints are consistent with the behaviour of the full-scale RC sections. Further testing at higher values of P would be desirable to more fully understand the behaviour of the model RC for applications; however, it should be noted that P = 400 kN represents 15% of the elastic critical load of the model sections as tested, which would represent close to an upper limit for axial force carried by columns in conventional building design.

5 SLOPE REINFORCEMENT USING VEGETATION

As an alternative to piles (and other 'hard' engineering solutions), using the roots of plants to stabilise slopes offers a number of potential benefits including: (i) being cheaper; (ii) requiring minimum specialist equipment for installation; (iii) an ability to sequester carbon dioxide (i.e. actively remove it from the atmosphere) rather than requiring CO_2 to be produced during manufacturing (for the steel and concrete in the piles); (iv) offer aesthetic and acoustic benefits from the above-ground part of the vegetation. These benefits can only be realised however if the roots are able to meet a similar level of performance to more traditional solutions.

As with the pile-reinforced slope case discussed in Section 2, there are competing geotechnical and 'structural' failure modes when using vegetation as

reinforcement. If the roots are strong enough, the most critical slip plane may deviate around the roots completely, normally moving into a deeper, less efficient position if the slope is uniformly planted across its face (Figure 13a). If the roots are weaker, the critical slip plane may pass through the rooted zone, with the roots failing either structurally in bending (which induces tensile strain within the roots) or in pull-out, depending on the relative soil-root strength (Figure 13b).

While the root soil interaction is elastic, the roots may be treated in the same way as piles such that the dimensionless group is essentially Equation 1. As it is rare and practically difficult to measure the bending stiffness of roots due to their high flexibility, it is useful to re-express Equation 1 idealising the root as a solid circular elastic element, i.e.

$$\frac{\eta L^4}{E_r D_r^3} \tag{11}$$

where E_r is the elastic stiffness (Young's Modulus) of the root and D_r is the root diameter. In a 1:N scale centrifuge test using the same soil in model and prototype, as η scales as N:1, E_r must therefore be scaled 1:1 to ensure similitude.

Continuing to treat the roots as analogous to solid-circular rods/piles (so that $Z_p = D_r^3/6$), combining Equations 2, 5 and 6 results in the second dimensionless group to be satisfied, representing relative soil-structure strength in shear/bending, for studying the ultimate limiting state:

$$\frac{K_p \gamma_s' L^3}{T_r D_r^2} \tag{12}$$

where T_r is the root tensile strength (used in place of f_y in Equation 6 if the root behaviour is idealised as elastic-perfectly plastic, i.e. $f_y = T_r$).

Equation 12 is most relevant for those roots in the root system which are close to vertical/perpendicular to the shear plane. There may, however, also be roots which are close to horizontal/parallel to the shear plane. This roots will be subjected to predominantly axial, rather than lateral loads, which suggests a further dimensionless group:

$$\frac{P_{pullout}}{P_{ult}} \tag{13}$$

where $P_{pullout}$ is the root pullout strength and P_{ult} is the root axial strength:

$$P_{ult} = T_r \cdot \frac{\pi D_r^2}{4} \tag{14}$$

The pullout strength may be estimated from the surface area multiplied by the normal effective stress multiplied by the root-soil interface friction coefficient (= tan δ'):

$$P_{pullout} = (\pi D_r L) \cdot (K \gamma_s' z) \cdot \tan \delta' \tag{15}$$

Where K is an appropriate earth-pressure coefficient to convert vertical effective stress into normal effective stress and δ' is the interface friction angle. Combining Equations 13 – 15 suggests that a suitable dimensionless group is:

$$\frac{K \tan \delta' \gamma_s' z L}{T_r D_r} \tag{16}$$

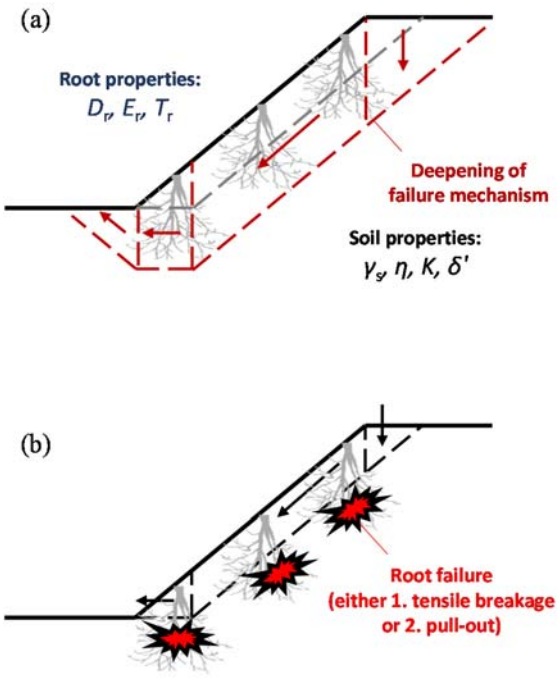

Figure 13 Failure mechanisms of a vegetation-reinforced slope: (a) soil fails around rooted zone; (b) roots fail.

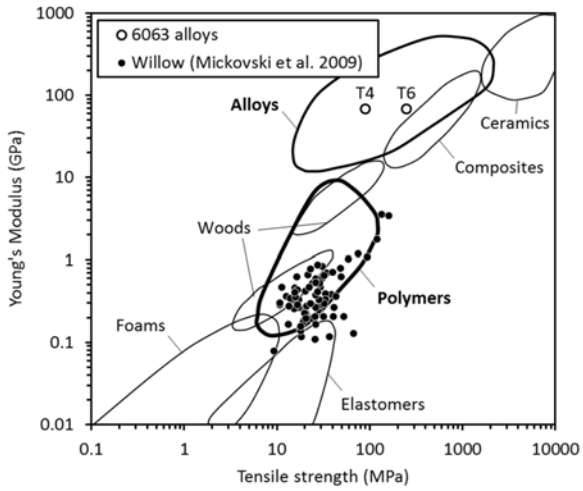

Figure 14 Identification of an analogue material for plant roots using a materials selection chart.

In a 1:N scale centrifuge test using the same soil in model and prototype, Equations 11, 12 and 16 can be scaled simultaneously if E_r and T_r are both scaled 1:1. The simplest way to achieve this would be to identify an existing and available material that has similar stiffness and strength as plant roots. Figure 14 presents a materials selection chart in which the properties of some willow roots measured by Mickovski et al. (2009) are shown relative to various common engineering materials (plotted as regions by material type). From Figure 14 it can be seen that polymers appear to represent a suitable class of materials. This is highly advantageous as many polymers can now be formed using stereo-lithography (commonly known as 3-D printing) which allows the complex architecture of root systems to be fabricated easily.

6 MODEL PLANT ROOTS

Once a suitable material has been identified for 3-D printing, it is only necessary to produce a 3-D model within computer-aided design (CAD) software which has a geometry and architecture representative of a live-plant root system. This cannot always be a direct reduced scale version of every root as some roots at small scale will be of a size which is too small for the printer to print (e.g. 0.75 mm is the smallest (threshold) diameter that can reliably be printed using the machine described in the following paragraph). Different approaches may be taken to producing an idealised geometry and these are discussed through two examples in this section.

Figure 15 shows a deep-rooting system that will be used in the centrifuge testing application described in Section 7. Figure 15a shows printed root models at 1:10 and 1:30 scales, with lines indicating the prototype depths of potential shear planes in the centrifuge (when tested at N = 10 and 30, respectively). These were printed using a Stratesys Inc. *uPrint SE* printer. The roots were designed in an artificial structure based on the sampled data of root cross-sectional area (CSA) for roots of different size classes in Figure 15b. The bars in this figure represent the printed models, while the line represents the total root CSA at depth for an Oak tree (*Quercus alba*) as reported in Danjon et al. (2008). For simplicity, the model uses just four different root diameters. Further information about the detailed design process and the shear strength contribution that the model can make within rooted soil can be found in Liang et al. (2017).

Figure 16 shows a different model for a Pine (*Pinus pinaster*) root system which has a greater amount of lateral rooting material. In this case, each individual root was digitised from the uprooted tree (as reported in Danjon et al. 2005) and the digital data is shown in Figure 16a. Figure 16b shows an isometric view of the digital idealisation of this root system at 1:20 scale in a form suitable for 3-D printing (the two

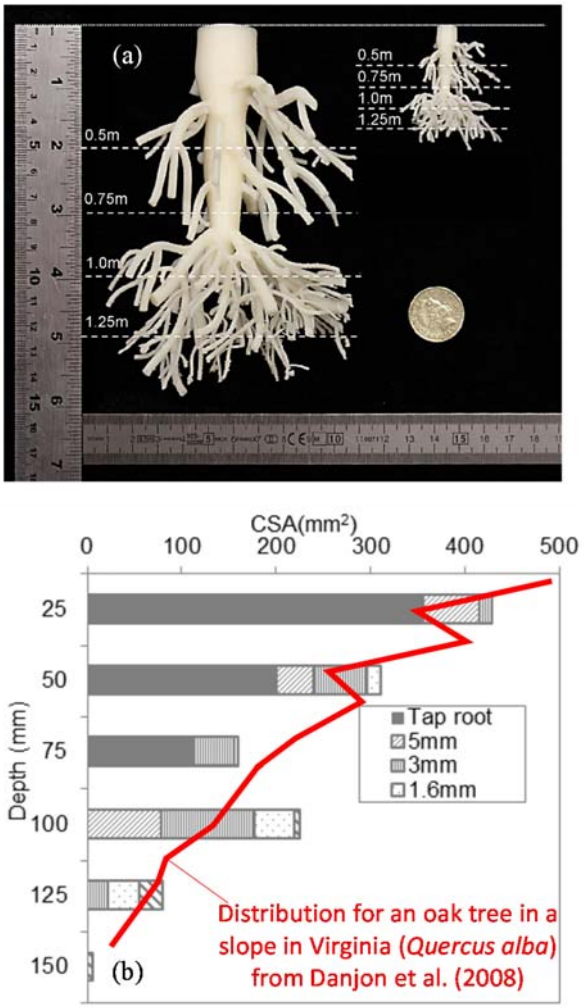

Figure 15 Artificially-created model root system produced using 3-D printing: (a) printed models at 1:10 and 1:30 scales; (b) root distribution data.

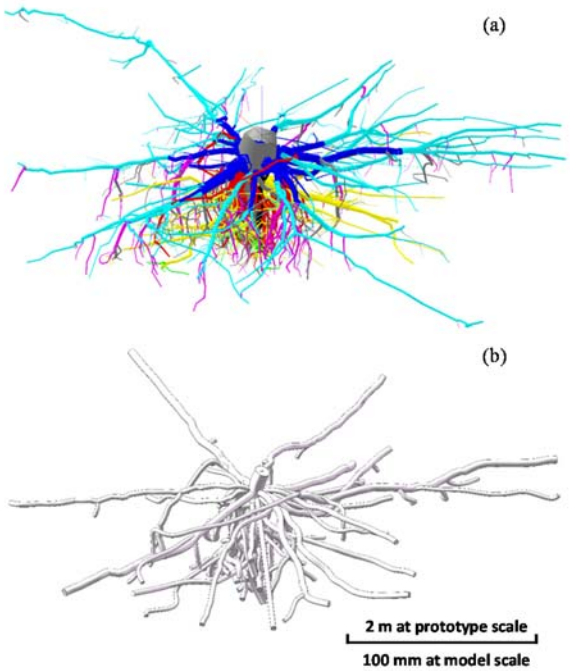

Figure 16 Model root system produced from digitised root data: (a) measured data; (b) idealised model at 1:20 scale.

figures are at the same scale as indicated in Figure 16b). In this case, the digital data for the root centrelines was directly imported into the CAD software Solidworks (i.e. as a wire-frame model) before diameters were assigned. Due to the minimum threshold diameter for printing, some of the finer root material could not be included; to compensate, some of the larger roots were slightly thickened to produce a model with the same overall root volume.

In each case, the roots were printed using an acrylonitrile Butadiene Styrene (ABS) filament, which has been shown to have representative E_r and T_r of plant roots by Liang et al. (2015), thereby satisfying Equations 11, 12 and 16.

7 APPLICATION – SEISMIC RESILIENCE

This section will demonstrate how the different types of reinforcement described in Sections 4 and 6 can be used to study the relative effectiveness of using plant roots as a low-carbon alternative to (RC) discrete piling for improving slope performance at an ultimate limiting state, using physical modelling. The case considered is of a slope which is statically stable (with a factor of safety of ~1.6) but in which movement may be induced due to the additional action from earthquake ground motion. Existing centrifuge test data will be collated and compared in which all of the aforementioned stiffness- and strength-related dimensionless groups have been satisfied for both types of reinforcement.

7.1 *Centrifuge testing*

A summary of the test arrangements considered can be found in Table 3. These consist of a series of pile reinforced cases (modelled at 1:50) where the piles are placed in a row midway between the crest and the toe at spacing, s, varying between $3.5 < s/B < 7.0$, and a vegetated case (modelled at 1:30) with 3-D printed analogue root clusters having the design described by Figure 15 placed at 1.4 m spacing (at prototype scale) in both horizontal directions (for a total of 36 clusters in the vegetated model).

Table 3 Centrifuge test data summary (all values at prototype scale).

Test ID	Method	Spacing	EI (MNm^2)	M_{ult} (kNm)
AA01	Unreinforced	N/A	N/A	N/A
AA13	Elastic piles	7.0B	50.4	3750
AA14	Elastic piles	4.7B	50.4	3750
AA15	Elastic piles	3.5B	50.4	3750
AA09	RC piles	7.0B	48.9	230
AA10	RC piles	4.7B	48.9	230
AA11	RC piles	3.5B	48.9	230
AA18	Weak RC piles	7.0B	42.2	70
TL05	Unreinforced	N/A	N/A	N/A
TL06	Vegetated	1.4 m	N/A	N/A

The model layouts are shown in Figure 17. Both models were instrumented with accelerometers within the soil, but this paper will focus only on the settlement at the crest of the slope (where transportation infrastructure may be situated), which is an indicator of the stability of the slope (as a higher yield acceleration due to reinforcement will result in less slip).

In the piled cases, both 'elastic' (aluminium-alloy type) and model RC piles are considered. The elastic cases have the model pile construction and properties given in Table 2 and Figures 4 and 5 and are instrumented with strain gauges at the positions indicated in Figure 4. The model RC piles are singly reinforced with $A_s/A_g = 0.85\%$ on the upslope side and shear reinforcement representative (at prototype scale) of a 13 mm diameter spiral at a pitch of 275 mm. For the case of $s/B = 7.0$, an additional model RC case was also considered, in which the reinforcement was not roughened with sand to represent the use of non-deformed reinforcing bar. The two model RC sections have reasonably similar EI, but the M_{ult} for the weak section is only 30% of that of the conventional model RC pile. In this sense, the weak pile may represent a pile with only nominal reinforcement, while the conventional model RC section is one that has been specifically designed to have a capacity greater than the induced bending moments (see later). The design of such a pile could be achieved straightforwardly in practice using the modified Newmark sliding block procedure for piled slopes presented by Al-Defae and Knappett (2015), which can estimate the maximum bending moment in the (elastic) piles for a given earthquake ground motion series.

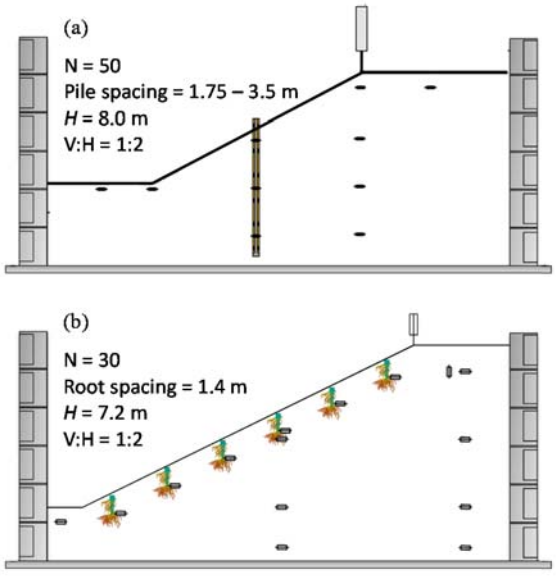

Figure 17 Centrifuge model layouts: (a) piled slopes; (b) vegetated slopes.

In both cases the soils were formed of dry sand at a relative density of 55% (to avoid liquefaction effects and as a model of a c′-ϕ′ soil). The slopes have an angle of 26.6° (vertical:horizontal = 1:2) and were formed within an equivalent shear beam container (ESB) to minimise dynamic wave reflection at the container boundaries. The slopes were of slightly different heights as indicated in Figure 17, though as the failure mechanism for the soil is very shallow and translational, they have the same static stability. They were also subjected to different earthquake time histories (using the QS67-2 servo-hydraulic earthquake simulator at the University of Dundee) and so results will be expressed in terms of the reduction in crest settlement compared to the unreinforced case. More detailed information on the modelling work, including details of the earthquake motions applied, may be found in Al-Defae and Knappett (2014) and Liang and Knappett (2017a).

7.2 *Comparative assessment of techniques*

A conventional stability analysis, conducted using available limit analysis methods could be undertaken to estimate the increase in the yield acceleration (k_{hy}) due to the presence of the reinforcement. Examples of how this may be done may be found in Al-Defae (2014) and Liang & Knappett (2017b). Such an analysis could be used to identify whether a design earthquake will trigger movement (e.g. for a return period of 475 years or 10% probability of exceedance with a 50 year design life). An increase in the yield acceleration (Δk_{hy}) by adding the reinforcement would allow a larger earthquake to be tolerated for the condition of no-slip (i.e. $k_{hy} \geq PGA_{design}$), which would extend the design life of the slope if the probability of exceedance of the design motion over the life of the slope was to be maintained.

However, it is becoming increasingly important to understand the resilience of engineering systems. In the case of a reinforced slope subjected to earthquakes, this involves considering the deformations which would occur if the design (no-slip) earthquake motion strength is exceeded, such that the implications for any supported infrastructure can be assessed. As both types of reinforcement considered here can model behaviour correctly into the inelastic range, centrifuge modelling can be used to investigate the performance when the earthquake motion is strong enough to induce slip. As an example, Figure 18 shows the response of the unreinforced and elastic pile reinforced slopes for s/B = 7.0. The earthquake motions used (from the 1999 Chi-Chi Earthquake in Taiwan with a peak ground acceleration of 0.41g) are strong enough to induce slip within the soil. This induces bending moments within the piles which in the elastic case are much less than M_{ult}.

Figure 19 compares the reduction in crest settlement (reinforced/unreinforced) for all of the test

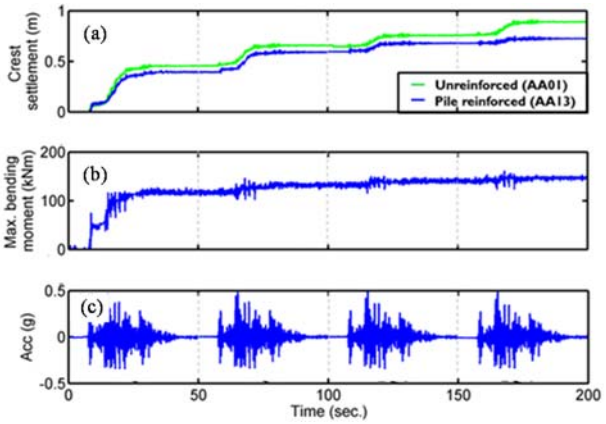

Figure 18 Measured response in elastic pile case for s/B = 7.0: (a) crest settlement; (b) maximum bending moment along the piles; (c) input ground motion.

cases. Comparing vegetation to the RC piles, it can be seen that for these similar slope heights, vegetation can provide a similar benefit to widely spaced RC piles. Comparing specifically the case at s/B = 7.0, the vegetation is similar in performance to the 'designed' pile and better than the RC pile with the nominal reinforcement. There is also evidence (Liang and Knappett 2017a) that in smaller slopes vegetation becomes much more effective (-85% reduction has been reported for a slope 2.4 m high). It may therefore be the case that for some slope heights, vegetation can significantly outperform conventional reinforcement, rather than matching it (further pile-reinforced tests are required to confirm this).

It is further evident from Figure 19 that the model RC piles perform differently from the elastic piles, even though the induced moments appear to be well below the M_{ult} of 230 kNm (Figure 18). Figure 20 shows the maximum induced moments in the piles

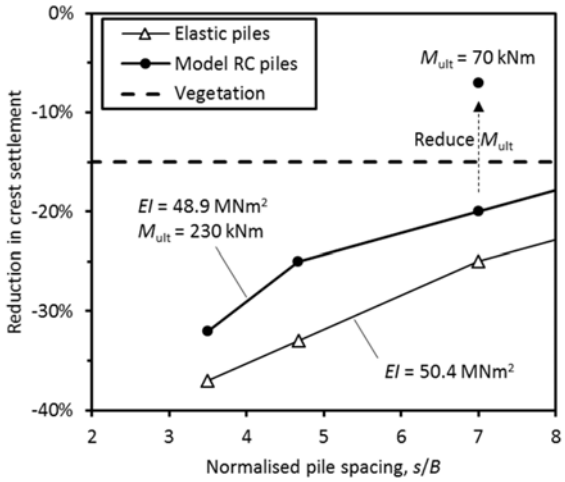

Figure 19 Comparative performance of piled and vegetated seismic slope reinforcement schemes.

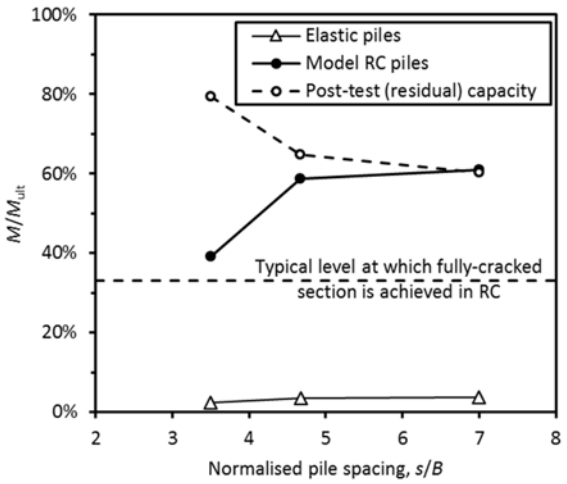

Figure 20 Proportion of pile bending capacity mobilised in pile-reinforced cases.

(assuming that the elastic pile measurements are representative also for the RC piles due to the similar *EI*) normalised by M_{ult} in each case. It can be seen that unlike the elastic piles which should be well within the truly elastic range ($M/M_{ult} < 5\%$) the RC piles mobilise a significant proportion of their capacity. The application of many cycles of loading at such high M/M_{ult} additionally results in a degradation in the residual capacity of the RC piles (measured from four-point bending tests of carefully exhumed piles from each test – three test piles per centrifuge test). This results in an even higher proportion of the instantaneous moment capacity being mobilised and explains the poorer performance of the RC piles compared to the elastic piles in Figure 19. This demonstrates the importance of developing models which can achieve similitude of stiffness and strength simultaneously, as the use of an elastic pile model would result in an overprediction of the resilience of the piled slope.

8 SUMMARY

Centrifuge modelling allows the constitutive behaviour of soils to be representative of full scale conditions when testing small scale models. However, for soil-structure interaction problems it is also important to appropriately model the behaviour of the structural elements. Dimensionless groups have here been developed to achieve this for piles and plant roots when used in soil reinforcement applications. Similar approaches could be developed for other types of reinforcement (e.g. retaining walls are similar to piles when loaded laterally, and soil nails are similar to plant roots, with structural and pull-out failure modes).

A range of possible techniques has subsequently been presented that can be used to achieve simultaneous similitude of both stiffness and strength to represent structural reinforcing elements made of steel or reinforced-concrete (RC), or plant roots. These are based upon various principles of material science, including metallurgical processes (heat treatment), behaviour of quasi-brittle materials (model RC) and the use of materials selection charts. This has been presented in the form of examples of model element design for centrifuge tests, and it is hoped that these worked examples will be useful to those learning centrifuge modelling.

Such models can be used with confidence when studying problems of soil-structure interaction at the ultimate limit state which is important for addressing topical issues such as assessing the resilience of old infrastructure against extreme events. An example of the application of the different modelling approaches was presented through an assessment of the potential for using vegetation as a low-carbon alternative to piles when used to increase the resilience of a slope to earthquake motions.

9 ACKNOWLEDGEMENTS

This paper is based on data collected by a number of researchers and students either formerly or currently at the University of Dundee, including: Dr Asad Al-Defae, Dr Teng Liang, Christine Reid, Patrick McDonnell and Kieran O'Reilly.

Thanks are also extended to Mark Truswell, Gary Callon, Colin Stark and Grant Kydd within the School of Science and Engineering for their assistance in fabricating the 3-D printed models, model formwork and beam/beam-column testing apparatus, and in running the centrifuge tests.

10 REFERENCES

Al-Defae, A. H. 2014. *Seismic performance of pile-reinforced slopes*. PhD Thesis, University of Dundee, UK.

Al-Defae, A. H. & Knappett, J. A. 2014. Centrifuge modelling of the seismic performance of pile-reinforced slopes. *J. Geotechnical & Geoenvironmental Engineering*, ASCE, 140(6): 04014014.

Al-Defae, A. H. & Knappett, J. A. 2015. Newmark sliding block model for pile-reinforced slopes under earthquake loading. *Soil Dynamics & Earthquake Engineering*, 75: 265-278.

American Concrete Institute (ACI) 2002. Building code requirements for structural concrete and commentary. *ACI 318-02*, American Concrete Institute, Farmington Hills, MI, USA.

Baker, W. M. & McMahon, T. F. 1969. Quality assurance in highway construction: Part 3 – Quality assurance of Portland Cement concrete. *Public Roads*, 35(8): 184-189.

Bažant, Z. P. & Yu, Q. 2005. Designing against size effect on shear strength of reinforced concrete beams without stirrups: II Verification and calibration. *Journal of Structural Engineering*, ASCE, 131(12): 1886-1897.

Belgin, C. M. & Sener, S. 2008. Size effect on failure of over-reinforced concrete beams. *Engineering Fracture Mechanics*, 75: 2308-2319.

British Standards Institution (BSI) 1992. Specification for aggregates from natural sources for concrete. *BS 882:1992*, London, UK.

British Standards Institution (BSI) 1997. Structural use of concrete – code of practice for design and construction. *BS 8110-1:1997*, London, UK.

Danjon, F., Barker, D. H., Drexhage, M. & Stokes, A. 2008. Using three-dimensional plant root architecture in models of shallow slope stability. *Annals of Botany*, 101(8): 1281-1293.

Danjon, F., Fourcaud, T. & Bert, D. 2005. Root architecture and wind-firmness of mature Pinus Pinaster. New Phytologist, 168: 387-400.

Elwood, K. J. & Eberhard, M. O. 2006. Effective stiffness of reinforced concrete columns. *PEER Research Digest No. 2006-1*, Pacific Earthquake Engineering Research Centre, University of California, Berkeley.

Florres-Berrones, R. & Whitman, R. V. 1982. Seismic response of end-bearing piles. *Journal of the Geotechnical Engineering Division*, ASCE, 108(GT4): 554-569.

Halstead, P. E. 1969. The significance of concrete cube tests. *Magazine of Concrete Research*, 21(69): 187-194.

Himsworth, F. R. 1954. The variability of concrete and its effect on mix design. *Proceedings of the Institution of Civil Engineers, Part I*, 3(2): 163-200.

Knappett, J. A. 2008. Discussion: Design charts for seismic analysis of single piles in clay, by A. Tabesh & H. G. Poulos. *Proceedings of the Institution of Civil Engineers, Geotechnical Engineering*, 161(GE2): 115-116.

Knappett, J. A., Reid, C., Kinmond, S. & O'Reilly, K. 2011. Small scale modelling of reinforced concrete structural elements for use in a geotechnical centrifuge. *Journal of Structural Engineering, ASCE,* 137(11): 1263-1271.

Kong, F. K. & Evans, R. H. 1987. *Reinforced and prestressed concrete*, 3rd Edition. E&FN Spon, London, UK.

Liang, T. Knappett, J. A. & Duckett, N. 2015. Modelling the seismic performance of rooted slopes from individual root-soil interaction to global slope behavior. *Géotechnique*, 65(12): 995-1009.

Liang, T., Knappett, J. A., Bengough, A. G. & Ke, Y. X. 2017. Small-scale modelling of plant root systems using 3D printing, with applications to investigate the role of vegetation on earthquake-induced landslides. *Landslides*, 14: 1747-1765.

Liang, T. & Knappett, J. A. 2017a. Centrifuge modelling of the influence of slope height on the seismic performance of rooted slopes. *Géotechnique*, 67(10): 855-869.

Liang, T. & Knappett, J. A. 2017b. Newmark sliding block model for predicting the seismic performance of vegetated slopes. *Soil Dynamics & Earthquake Engineering*, 101: 27-40.

Litle, W. A. & Paparoni, M. 1966. Size effect in small scale models of reinforced concrete beams. *Journal of the American Concrete Institute*, 63(11): 1191-1204.

Loli, M., Knappett, J. A., Brown, M. J., Anastasopoulos, I. & Gazetas, G. 2014. Centrifuge modeling of rocking-isolated inelastic RC bridge piers. *Earthquake Engineering & Structural Dynamics*, 43: 2341-2359.

Madabhushi, S. P. G. 2014. *Centrifuge Modelling for Civil Engineers*. CRC Press, Boca Raton FL, USA.

Mansur, M. A. & Islam, M. M. 2002. Interpretation of concrete strength for non-standard specimens. *Journal of Materials in Civil Engineering*, ASCE, 14(2): 151-155.

Mickovski, S. B., Hallett, P. D., Bransby, M. F., Davies, M. C. R., Sonnenberg, R. & Bengough, A. G. 2009. Mechanical reinforcement of soil by willow roots: Impacts of root properties and root failure mechanism. *Soil Science Society of America Journal*, 73(4): 1276-1285.

Neville, A. M. 1959. The relation between standard deviation and mean strength of concrete test cubes. *Magazine of Concrete Research*, 11(32): 75-84.

Wood, D. M. 2004. *Geotechnical Modelling*. Spon Press, Abingdon, UK